HIGH-FREQUENCY GROUND MOTION SCALING IN THE YUNNAN REGION

Winston Chan,[1] Robert Herrmann,[2] and Wenjie Jiao[1]

Multimax Inc.,[1] Saint Louis University[2]

Sponsored by Defense Threat Reduction Agency

Contract No. DTRA01-00-C-0068

ABSTRACT

Vertical component velocity seismograms from the Yunnan digital seismic provincial network are used to characterize high-frequency S-wave propagation. The signals are processed to examine the peak ground motion and Fourier velocity spectra in the frequency range of 1 - 12 Hz. Analysis involves a two-step process: first, modeling of peak S-wave motions in terms of EXCITATION, DISTANCE, and SITE terms; this is followed by a parameterization in terms of geometrical spreading, frequency dependent Q and distance-dependent duration. The data set consists of over 6000 waveforms from 23 stations and 325 events. Observations are in the distance range of 30 - 700km. The data are processed for purposes of defining the parameters needed for the application of Random Vibration Theory to predict high-frequency earthquake motions.

OBJECTIVE

Introduction

The Lg/Pg ratio has been shown to improve discriminant performance as the frequency content increases, with frequencies higher than 5 Hz leading to good separation of explosion and earthquake populations in most regions where it has been tested (National Research Council, 1997). For example, in their study of discrimination between Nevada Test Site (NTS) explosions and earthquakes, Walter *et al*. (1995) noted improved performance at higher frequencies. Other examples are the regional discrimination study of explosions and earthquakes in the eastern United States and in southern Russia by Kim *et al*. (1997), who observed significantly improved discrimination capability of the amplitude ratio P/Lg in the 5- to 25-Hz band over the lower frequency bands. Several recent studies (e.g., Baumgardt and Schneider, 1997; Rodgers and Walter, 1997; Walter *et al.* 1997) have observed significant variability of regional phase ratios, such as Pn/Lg or Pg/Lg, which are generally powerful regional discriminants. Their characteristics vary significantly from one tectonic or geographic region to another and may also be strongly dependent on frequency (e.g. Baumgardt and Der, 1994). Southwestern China is known to have complex geology with large Q variations (e.g. Qin and Kan, 1986), so that several combinations of distinct source and receiver regions will need to be calibrated. It is important to understand and quantify these differences in order to accomplish improved regional discrimination in a region of complex geology, such as the Yunnan Province in southwestern China.

In order to systematically perform the spectral ratio study, we have to apply the magnitude and distance corrections to the signals. We propose to apply the techniques for characterizing high-frequency S-wave motion to improve the effectiveness of the regional seismic discriminants and extend the application to P-wave also. The procedures used in the analysis were developed by Yazd (1993) and then extended to the current processing and interpretation described in Raoof *et al* (1999) and Malagnini (1999). At present the central US, southern Great Basin surrounding NTS, southern California, the US Pacific Northwest, Italy, and Germany have been studied using the same methodology. Studies on Switzerland, Utah, Valle de Mexico, and Turkey are underway or just starting. The goal of processing to date is to use regional network data in Yunnan Province from small to moderate earthquakes to constrain ground motion estimates for large earthquakes. Data analysis consists of processing a very large set of waveforms (~1000-2000) distributed uniformly from short to large distances to characterize the high-frequency motion. The result of this analysis is an empirical *D(r)*, *Site* and *Excitation* term.

RESEARCH ACCOMPLISHED

Data Collection and Processing

We have constructed a large database of short-period waveform data from the Yunnan regional network in southwestern China. Figure 1 shows the event location and stations used for the analysis of high-frequency ground motion. A prerequisite for successful regression is the requirement for each station to observe events at different distances, and that each event be observed by many stations with overlapping distance distributions, as shown in Fig. 2. This is required for the data to define the actual distance dependence of motion independently of station site/instrument effects.

The specifics of the Regression Model are:

- Use filtered vertical component velocity at 1, 2, 3, 4, 6, 8, 10 and 12 Hz (DT = 0.02 s)
- Use Coda normalization as an independent test of distance term.
- Perform regression on Peak Velocities and Fourier Velocity Spectra at each frequency for the model $\log A = D(r) + E(r_{ref}) + S$

where A is observed motion, $D(r)$ is distance term, $E(r_{ref})$ is the excitation term at the reference distance, and S is a site term, and the following constraints apply: $\Sigma Si = 0$; $D(40\ km) = 0$; $D(r)$ is a piecewise linear continuous function defined by distance nodes. A smoothing constraint is applied to $D(r)$.

Stable regression requires a non-singular set of equations. The data define the actual distance variation. A reference distance is chosen to be within the range of observed distances. This reference distance is chosen to be 40 km, which is large enough that errors in hypocentral distance due to poor event depths will not be important and is less than the distance at which supercritical reflections from the Moho become important. The net effect of these constraints indicates that the $E(r_{ref})$ is the network average motion at that distance. The $D(r)$ then corrects that level of motion

to the desired distance and the $S(f)$ term provides a local correction for a site for component of motion. Regression results for processing the peak S motion at 1.0 Hz are shown in Fig. 3. The uniform distribution of residuals and the lack of significant outliers indicate uniform calibration of instruments. The distance distribution indicates that the regression can only constrain high-frequency motion in the 30- to 800-km distance range.

To indicate the frequency dependence of D(r), the regression is performed separately at each frequency under the constraint that D(r) = 0 at r = 40 km (Fig. 4). Because of the lack of data at short distances, curves are not plotted for r < 30 km. Given the excitation at 40 km, this figure is used to predict the level of motion at other distances as a function of frequency. This figure is for the regression of filtered peak velocities. A similar figure results from the regression of the Fourier velocity spectra observations.

Duration is defined as the length of time that bounds the 5% and 75% bounds of $TS\int s(t)2dt$. The Fourier velocity spectra are generated from the signal within this window, and the combination of the spectra and duration are used with Random Vibration Theory to predict the peak motion. Fig. 5 shows all durations whose corresponding observed peak motion are within the 5-95% range of predicted values. There are still outliers at large distances. A least-squares estimate of duration is plotted on top of the observations. Outliers affect the least squares estimate, and hence the regression curve deviates from the dense trend of observations at large times. The increase of duration with distance is related to crustal structure. Fig. 6 shows the comparison of distance dependence for the various frequencies. The durations for frequencies > 1.0 Hz are very similar, whereas the duration at 1.0 Hz is greater at shorter distances. This may be due to the fact that the 1.0-Hz signal contains scattered surface waves at the lowest frequency.

Modeling

The predicted Fourier velocity spectra for a frequency f and a distance r is:

$$a(r,f) = s(f,\mathbf{M}_W)g(r)\tilde{e}^{\pi f r/Q(f)}\,\beta V(f)\tilde{e}^{\pi f\kappa_0}$$

where $a(r,f)$ is the Fourier velocity spectra, $s(f,\mathbf{M}_W)$ is the source excitation as a function of moment-magnitude, $g(r)$ is the geometrical spreading function, $Q(f)$ is the frequency dependent quality factor, which equals $Q_0(f/1.0)^{\eta}$, Q_0 is the quality factor at 1.0 Hz, $V(f)$ is a frequency dependent site amplification, and κ_0 controls site dependent attenuation of high frequency. This is a phenomenological description that conceptually includes everything that affects the observed signal. Usually little is known about the site and the *V((f)exp(-* $\pi f\kappa$*)* is lumped together as a *exp(-* $\pi f\kappa_{eff}$*)*term as a simplification which is valid since this a reasonable approximation over the limited frequency band of observations.

A comparison to the regression model shows the following correspondence for the Fourier Velocity spectra:

$$10E = s(f,\mathbf{M}_W)g(r_{ref})\tilde{e}^{\pi f r_{ref}/Q(f)}\,\beta V(f)\,\tilde{e}^{\pi f\kappa_0}$$
$$10D = g(r)\tilde{e}^{\pi f r/Q(f)}\,\beta g(r_{ref})\tilde{e}^{\pi f r_{ref}/Q(f)}\,\beta$$
$$10Si = V(f)\,\tilde{e}^{\pi f\kappa_0}V(f)\tilde{e}^{\pi f\kappa_0},$$

where $V(f)\,\tilde{e}^{\pi f\kappa_0}f$ is the network average site effect arising from the $\sum Si = 0$ constraint. This interpretation is tied to the constraints used in the inversion: the use of a reference distance and the $\sum Si = 0$ constraint.

The modeling procedures include:

Model Fourier Velocity. Start with $g(r)$, Q_0 and η. Next look at small event E terms to get κ_0.
Include duration to model time domain $D(r)$. Compare observed and predicted $D(r)$'s. Compare observed and predicted $E(r_{ref},f)$'s.

Use events with known M_W to constrain the $g(r)$ from the source to the first observation distance, here about 40 km. The initial effort is to model the *D(r)* term in terms of the *g(r)* and the *Q(f)*. The rationale is that these terms are separable for the Fourier Velocity and approximately so for the time domain observations. Once these are defined, only the source spectrum and the site term affect the observed level of motion at the reference distance. For $M_W <$ 2.5, the source spectrum is independent of stress drop in the frequency range of 1 - 12 Hz for stress drops > 50 bars

or so. Thus, only the site term affects the unmatched part of the $E(r_{ref})$. Note we cannot separate the effect of the site term from the source spectrum; we do so for convention. It may be possible to see different site terms with some data sets (New Madrid) by comparing the *E()* functions for ΣSZ = 0 and ΣSH = 0 regressions. The real unknown is the *g(r)* required to get the motion from the source to the first observation distance. This is usually assumed to be of the form r^{-1} - but synthetic seismogram modeling indicates that the decay may be slightly more rapid. If we independently have an M_W and have sufficient observations at lower frequencies so that unknown stress drop does not affect us, we can use this additional evidence to define the proper g(r) for distances outside our observations.

Comparison of model fit to the Fourier velocity excitation terms is shown in Fig. 7. The high-frequency level for small events is not a function of stress drop. The largest events in the data set had moment magnitudes of 5 - 5.5. The averages are used to be able to see the trends. Comparison of model fit to the Fourier velocity *D(r)* term is shown in Fig. 8. To highlight the frequency dependence, the deviation from a *1/r* trend is plotted. Remember data only for r > 30. Fig. 9 shows the comparison of model fit to the filtered time domain velocity *D(r)* term. To highlight the frequency dependence, the deviation from a *1/r* trend is plotted. Remember data only for r > 30.

Model Parameters:

k_0 = 0. 050 *s; Q*(*f*) = 200(*f* /1. 0)0.49; *VS*(for*Q*) = 3. 5 *km*/*s; VS*(*source*) = 3. 5 *km*/*s;*
r= 2. 8 *gm*/*cm*3; *f*max = 100 *Hz;* Δs= 100 *bars; V*(*f*) = 1.0

$$g(r) = \begin{cases} r1 & 1\ km \le r \le 40 km \\ r1.2 & 40\ km \le r <= 90\ km \\ r0 & 90\ km \le r \le 150\ km \\ r0.5 & R \le 150\ km \end{cases}$$

$$T(r) = \begin{cases} s & r = 0\ km \\ 5\ s & r = 50\ km \\ 8\ s & r = 200\ km \\ 15\ s & r = 500\ km \\ 18\ s & r = 1000\ km \end{cases}$$

In performing the regression, the site term constraint can be taken to be ΣZ = 0, with no constraint on the horizontal components. This means that both the vertical and the horizontal data constrain the *D(r)* term, but only the vertical components define the *E(r)*. We can now form the *log H/Z* ratio subtracting the horizontal S term from the corresponding vertical at a station (Fig. 10). The ratio depends on the earth model and predominant focal mechanism. Any frequency dependence would be indicative of very strong site effects that are seen in this data set. We see that log(H/Z) ˜ 0.2 for this data set. Fig. 11 shows the plot of site terms for the regression on peak-filtered motions. A positive site term represents a motion greater than expected for the network average. This could be due either to an actual size effect due to local structure or to absolute instrument calibration.

CONCLUSIONS AND RECOMMENDATIONS

This study indicates that modeling of small event distance dependence and excitation terms is independent of stress drop and source scaling and the modeling of large events requires a source model. Moments from larger events are needed to further constrain *g*(*r*) and *S*(*f*). This study has provided constraints on the amplitude-distance relation of 1- to 12-Hz high-frequency ground motion in the distance range of 30 - 600 km in Yunnan and surrounding provinces. More work is required on the absolute scaling of ground motion in terms of the source. We hope to use waveform modeling to define focal mechanisms, source depths and seismic moments for many of the larger events. This may help define the correct geometrical spreading from the source to the first observations at 30 km and also constrain the stress drop of these events. This study is an important first step in predicting ground motion for large magnitude earthquakes in the region.

REFERENCES

Baumgardt, D. R. and Z. A. Der (1994), Investigation of the transportability of the P/S ratio discriminant to different tectonic regions, PL-TR-94-2299, Phillips Laboratory, Hanscom Air Force Base, Massachusetts.

Baumgardt, D. R. and C. M. Schneider (1997), Multivariate canonical correlation of P/S ratios and propagation path parameters for Iran, *Proc. 19th Annual Seismic Research Symposium on Monitoring a Comprehensive Test Ban Treaty* (Editors: M. J. Shore, R. S. Jih, A. Dainty, and J. Erwin), Defense Special Weapons Agency, Alexandria, 14-23.

Kim, W. Y., V. Aharonian, A. L. Lerner-Lam, and P. G. Richards (1997), Discrimination of earthquakes and explosions in southern Russia using regional high-frequency three-component data from the IRIS/JSP Caucasus Network, *Bull. Seism. Soc. Am* **87***,* 569-588.

Malagnini, L. (1999), Ground Motion Scaling in Italy and Germany, *Ph. D. Dissertation*.

National Research Council (1997), Research Required to Support Comprehensive Test Ban Treaty Monitoring, National Academy Press, Washington, D.C.

Qin, J. Z. and R. J. Kan (1986), Q Values and Seismic Moments Estimates Using the Coda Waves of Near Earthquakes in the Kunming and Surrounding Regions, *Chinese J. Geophy*., **29**(2): 145-155.

Raoof, M., R. B. Herrmann, and L. Malagnini (1999), Attenuation and excitation of three-component ground motion in Southern California, *Bull. Seism. Soc. Am.* **89**, (Aug. 99) preprint.

Rodgers, A. and W. Walter (1997), Regionalization and calibration of seismic discriminants, path effects, and signal-to-noise for station ABKT, *Proc. 19th Annual Seismic Research Symposium on Monitoring a Comprehensive Test Ban Treaty* (Editors: M. J. Shore, R. S. Jih, A. Dainty, and J. Erwin), Defense Special Weapons Agency, Alexandria, 143-151.

Walter, W. R, K. M. Mayeda, and H. J. Patton (1995), Phase and spectral ratio discrimination between NTS earthquakes and explosions. Part1: empirical observations, *Bull. Seism.Soc.Am* **85**, 1050-1067.

Walter, W. R., D. B. Harris, and S. C. Myers (1997), Seismic discrimination between earthquakes and explosions in the Middle East and North Africa, *Proc. 19th Annual Seismic Research Symposium on Monitoring a Comprehensive Test Ban Treaty* (Editors: M. J. Shore, R. S. Jih, A. Dainty, and J. Erwin), Defense Special Weapons Agency, Alexandria, 459-468.

Yazd, M. R. S. (1993), Ground motion studies in the Southern Great Basin of Nevada and California, *Ph. D. Dissertation*, Saint Louis University, 189p.

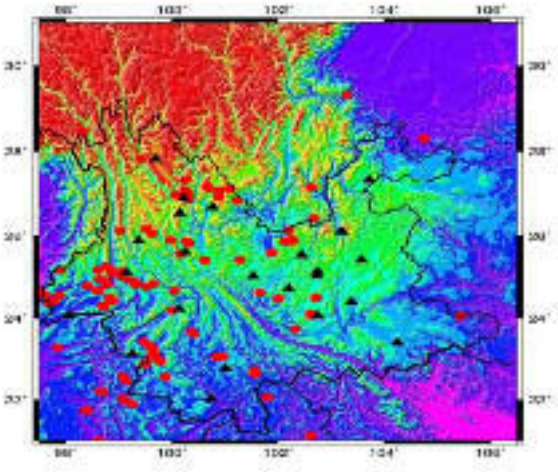

Figure 1. Plot of events, left, and stations, right, used for the analysis of high frequency ground motion in the Yunnan region of southwestern China.

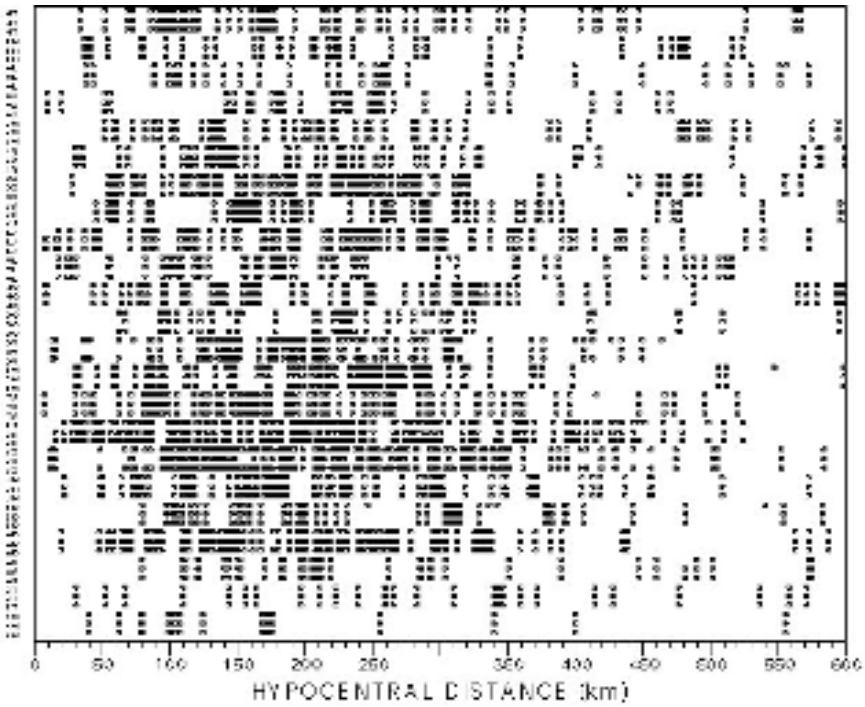

Figure 2. Distribution of observed events for each station at different distances indicates that each event can be observed by many stations, and that the distance distributions overlap.

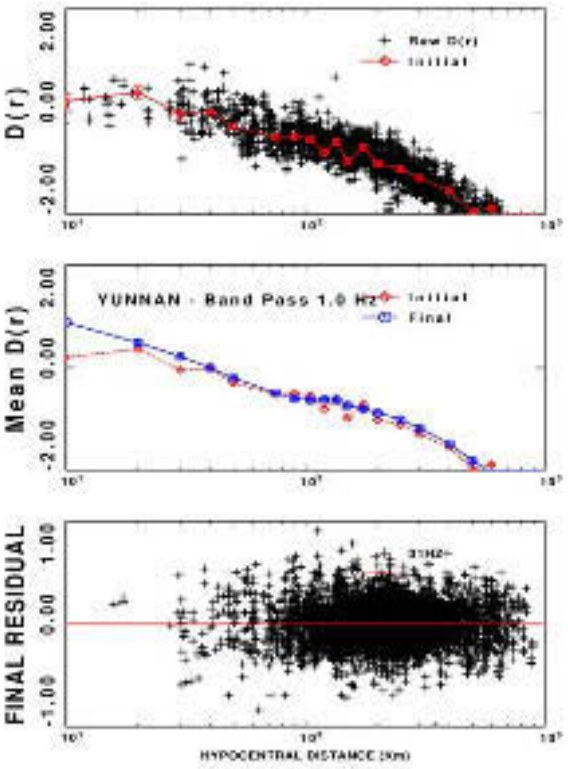

Figure 3. Regression results for processing the peak S motion at 1.0 Hz. top). Estimate of the D(r) term using the coda normalization technique; middle), Comparison of coda normalization (red) and regression (blue) results; bottom) regression residuals as a function of distance.

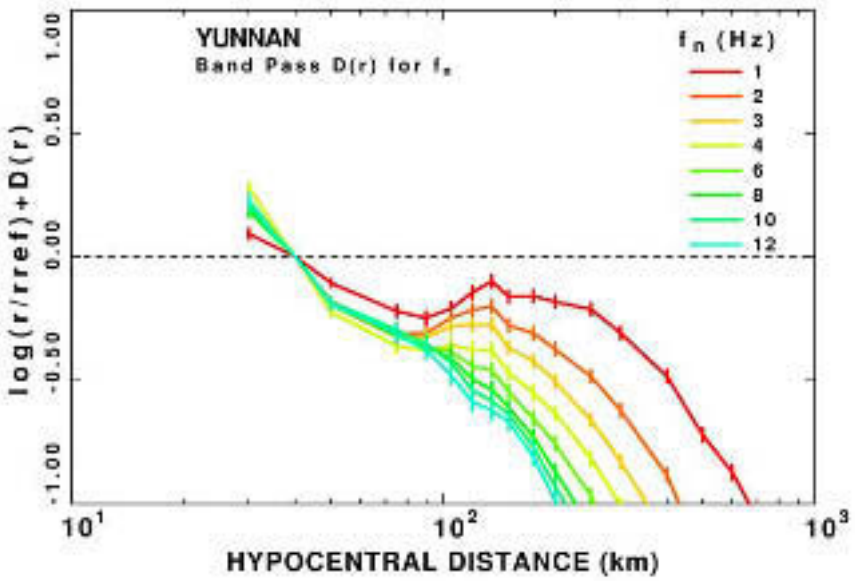

Figure 4. This figure compares the D(r) for each frequency of the regression of filtered peak velocities. Because of the lack of data at short distances, curves are not plotted for r < 30 km.

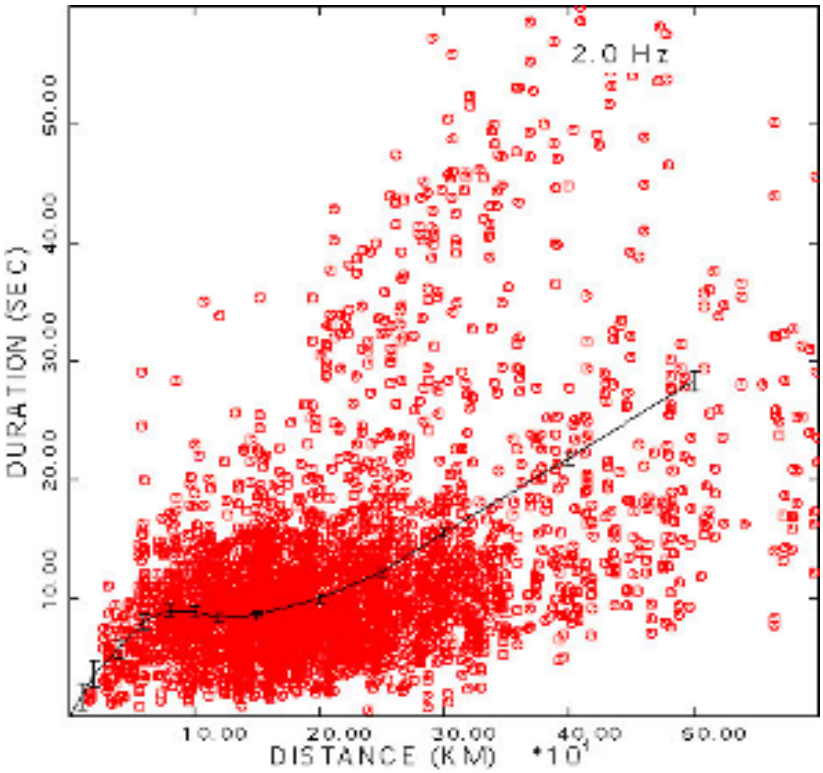

Figure 5. Distance Dependent Duration for a frequency of 2 Hz. A least-squares estimate of duration is plotted on top of the observations.

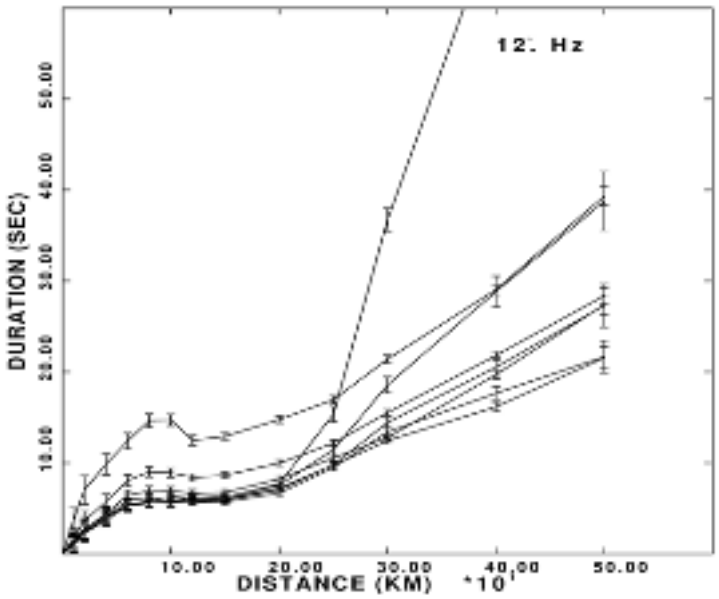

Figure 6. Comparison of duration versus distance at various frequencies.

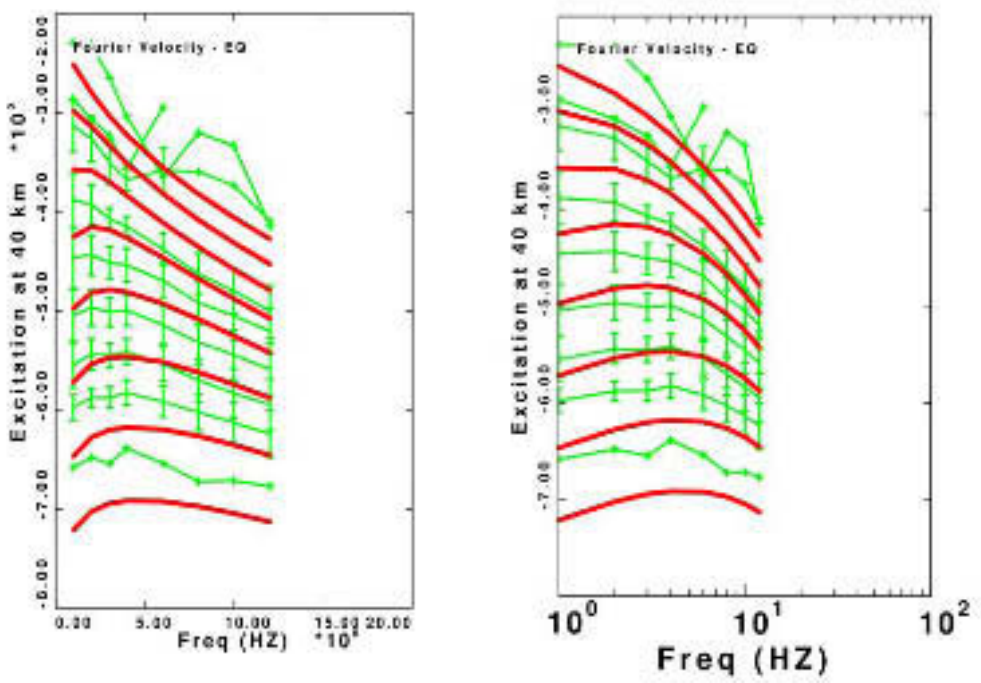

Figure 7. Comparison of model fit to the Fourier velocity excitation terms. The green lines are averages of the regression excitation terms into groups that are separated by 0.5 log units in level at 3.0 Hz. The red curves are the predicted excitation terms for the model for moment magnitudes of 2.0 - 5.5 at increments of 0.5 moment magnitude units.

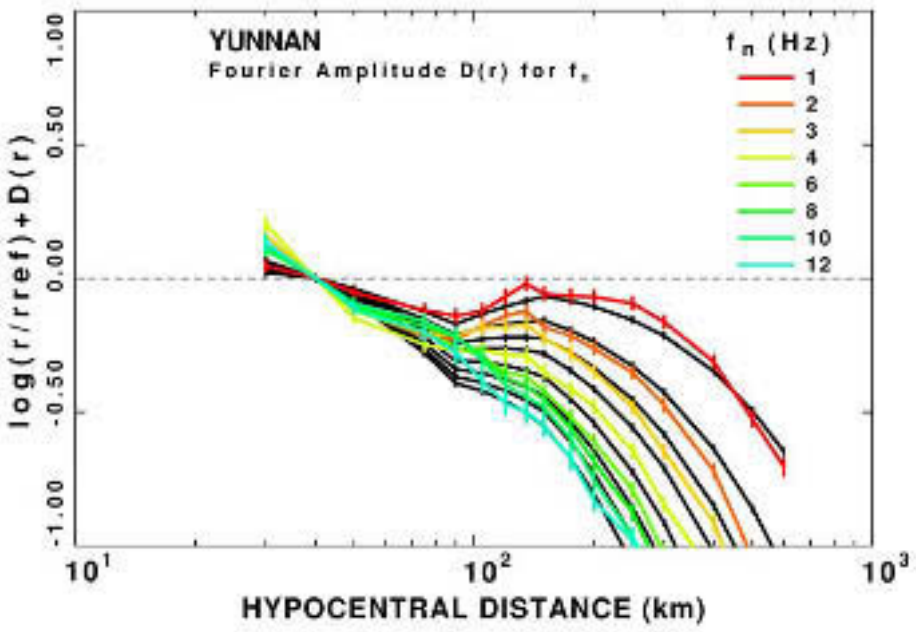

Figure 8. Fourier D(r): Comparison of model fit to the Fourier velocity *D(r)* term. The regression results (color) are plotted on top of the predicted values (black). To highlight the frequency dependence, the deviation from a *1/r* trend is plotted. Remember data only for r > 30.

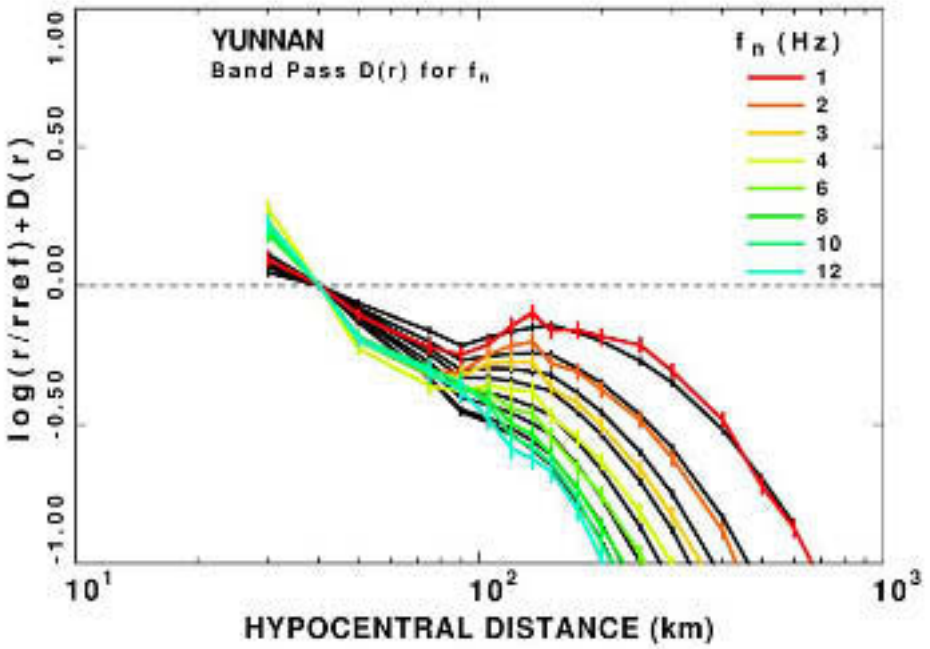

Figure 9. Comparison of model fit to the filtered time domain velocity *D(r)* term. The regression results (color) are plotted on top of the predicted values (black). To highlight the frequency dependence, the deviation from a *1/r* trend is plotted.

H/Z Ratio

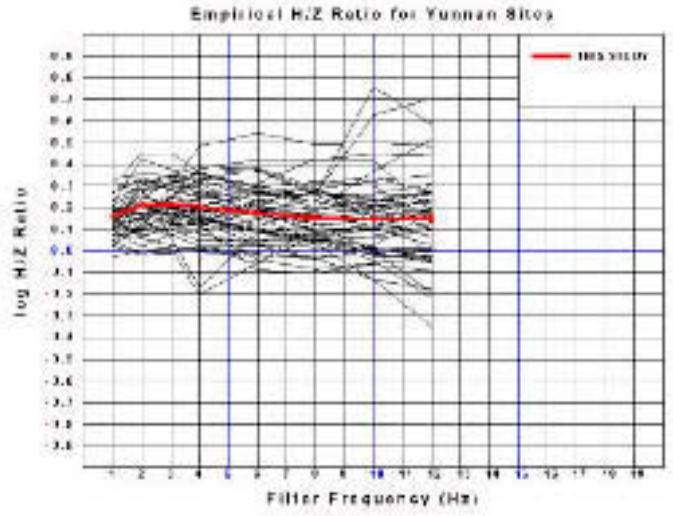

Figure 10. H/Z Ratio: In performing the regression, the site term constraint can be taken to be □Z = 0, with no constraint on the horizontal components. The ratio depends on the earth model and predominant focal mechanism. Any frequency dependence that would be indicative of very strong site effects are seen in this data set.

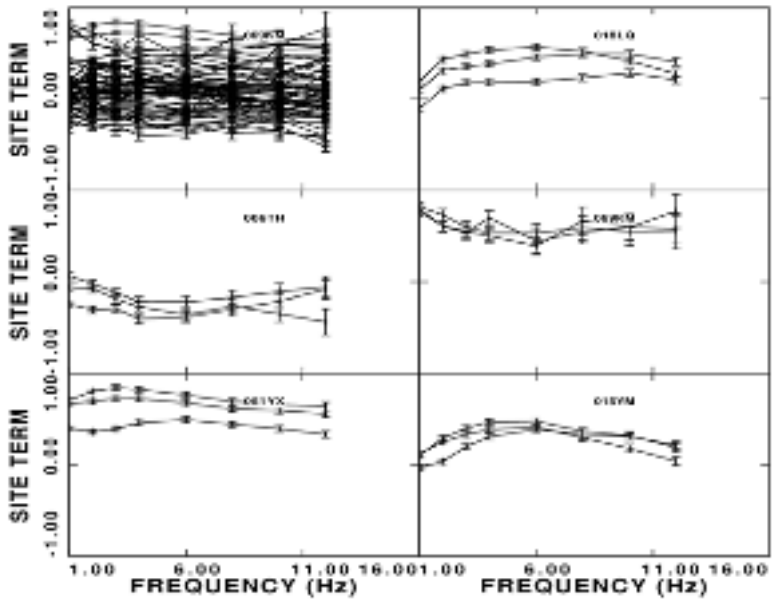

Figure 11. Plot of site terms for the regression on peak-filtered motions. Site terms for all components are plotted at the upper left. The remaining panels display the site terms for selected stations with large deviations from 0.